Materials Research Express

PAPER • OPEN ACCESS

Revisiting the layered $Na_3Fe_3(PO_4)_4$ phosphate sodium insertion compound: structure, magnetic and electrochemical study

To cite this article: Ganesh S Shinde *et al* 2020 *Mater. Res. Express* **7** 014001

Materials Research Express

PAPER

Revisiting the layered $Na_3Fe_3(PO_4)_4$ phosphate sodium insertion compound: structure, magnetic and electrochemical study

Ganesh S Shinde[1], **Ritambhara Gond**[1], **Maxim Avdeev**[2,3], **Chris D Ling**[3], **Rayavarapu Prasada Rao**[4], **Stefan Adams**[5] **and Prabeer Barpanda**[1]

[1] Faraday Materials Laboratory, Materials Research Center, Indian Institute of Science, C. V. Raman Avenue, Bangalore 560012, India
[2] Bragg Institute, B87, Australian Nuclear Science and Technology Organization, Locked Bag 2001, Kirrawee DC NSW 2232, Australia
[3] School of Chemistry, The University of Sydney, Sydney, NSW 2006, Australia
[4] Centre for Materials for Electronics Technology, Pune 411008, Maharashtra, India
[5] Department of Materials Science and Engineering, National University of Singapore, 9 Engineering Drive 1, Singapore 117546, Singapore

E-mail: prabeer@iisc.ac.in

Keywords: Na-ion batteries, cathode, $Na_3Fe_3(PO_4)_4$, layered structure, BVSE calculation

OPEN ACCESS

RECEIVED
10 October 2019

REVISED
26 October 2019

ACCEPTED FOR PUBLICATION
6 November 2019

PUBLISHED
18 November 2019

Abstract

Layered sodium iron phosphate phase [$Na_3Fe_3(PO_4)_4$] was synthesized by solution combustion synthesis method, marking the first attempt of solvothermal synthesis of this phase. Its crystal structure was verified by synchrotron and neutron powder diffraction. Rietveld analyses proved the phase purity and formation of monoclinic framework with $C2/c$ symmetry. It undergoes an antiferromagnetic ordering ~27 K. This combustion prepared nanoscale $Na_3Fe_3(PO_4)_4$ compound was found to be electrochemically active with a stepwise voltage profile involving an Fe^{3+}/Fe^{2+} redox activity centred at 2.43 V vs. Na/Na^+. Despite various cathode optimization, only 1.8 Na^+ per formula unit could be reversibly inserted into the $Na_3Fe_3(PO_4)_4$ framework leading to capacity close to 50 mAh g^{-1}. This limited electrochemical activity can be rooted to (i) relatively large diffusion barrier (ca. 0.28 eV) as per Bond valence site energy (BVSE) calculations and (ii) possible structural instability during (de)sodiation reaction.

1. Introduction

With industrial and technological evolution, global energy consumption is increasing at a very high rate. In this scenario, energy generation with minimal CO_2 emission is pivotal. Also, efficient energy storage and delivery is a key sector propelling myriads of consumer electronics, (hybrid) electric vehicles and stationary micro-to-mega grid storage in the 21st century. While several technologies do exist, electrochemical energy storage in general and rechargeable batteries in particular offer the most pragmatic approach with feasible large-scale dissemination. In the last three decades, rechargeable Li-ion batteries have seen unprecedented commercialization ushering a wireless revolution and vying for zero-emission transportation. Batteries with good combination and energy/power density, reversibility, safe operation and materials/process economy are crucial to meet the demand of the energy-hungry world [1, 2]. From application point of view, batteries can be divided into two categories: volume/weight restricted portable batteries and volume/weight independent stationary batteries. While the former is solely dominated by Li-ion chemistry, the latter category can be catered by alternate chemistry like lead-acid, Ni-MH, Li-ion as well as Na-ion batteries.

While the Li-ion and Na-ion batteries work on similar operating principles, sodium-ion batteries are touted as economic alternatives to Li-ion counterparts owing to the elemental abundance and uniform geographic distribution of sodium-based precursors. Similar to the story of Li-ion batteries, successful implementation of Na-ion batteries relies a lot on robust positive insertion (cathode) materials. Over the last decade, Na-ion batteries have attracted significant research effort to develop new cathode materials, where layered transition metal oxides ($Na_xT_MO_2$, T_M = Co, Fe, Mn, Cr etc) have ruled the field ever since their discovery in 1980s [3–8]. However, these layered have issues with structural and thermal stability. To circumvent these issues, many a polyanionic insertion materials have been unravelled. While the theoretical capacity (Q_{Th}) is lower owing to high

molecular weight, using inductive effect principle, superior operating voltage can be realized leading to competitive energy density [9, 10]. Among these polyanionic materials, while the SO_4^{2-}-based compounds offer the highest redox voltage [11, 12], the PO_4^{3-}-based ones render easy synthesis and materials stability [13].

Exploring the phosphate chemistry, various polyanionic cathodes have been reported such as $NaFePO_4$, $NaVPO_4F$, $Na_3V_2(PO_4)_2F_3$, Na_2FePO_4F, $Na_2FeP_2O_7$, $Na_4Fe_3(PO_4)_2(P_2O_7)$ etc [6]. One such PO_4-based cathode system is $Na_3Fe_3(PO_4)_4$, a layer structured sodium iron phosphate [14, 15]. It offers suitable channels for Na^+ ion insertion between the layers built from corner-sharing FeO_6 octahedra and PO_4 tetrahedra [16], with a theoretical insertion ability of 3 Na per formula unit. However, the previous report realized the reversible intercalation of only 1.8 Na^+ ions per formula unit of $Na_3Fe_3(PO_4)_4$ framework, that too in very low current rage of C/100 (1 Na^+ in 100 h) [14]. The layered structure and high theoretical capacity based on 2 electron transfer motivated us to re-examine and optimize this compound to achieve better electrochemical performances.

In this current work, we have synthesized $Na_3Fe_3(PO_4)_4$ framework via wet chemistry route for the first time. Its crystal structure was analysed combining synchrotron and neutron powder diffraction. $Na_3Fe_3(PO_4)_4$ exhibits layered structure assuming a monoclinic system with $C2/c$ symmetry. Solution route leads to smaller particles with improved electrochemical reversible capacity of 50 mAh g^{-1} at a faster rate of C/20 involving a 2.45 V Fe^{3+}/Fe^{2+} activity. Despite particle size optimization and carbon coating, it was impossible to obtain near theoretical capacity. Here, we report the wet chemical synthesis, structure, magnetic and electrochemical properties of as-synthesized $Na_3Fe_3(PO_4)_4$. The Na^+ migration and diffusional analysis has been calculated to probe the reason behind electrochemical limitations.

2. Experimental

2.1. Materials synthesis

The target compound $Na_3Fe_3(PO_4)_4$ was synthesized via wet chemistry route for the first time. The wet chemical synthesis was carried out with or without using fuels such as glycine ($C_2H_5NO_2$, 99%, Merck), urea (CH_4N_2O, 99%, SDFCL) and ascorbic acid ($C_6H_8O_6$, 99%, Sigma Aldrich). Stoichiometric quantities of $NaH_2(PO_4).H_2O$ (99%, EMPARTA.ACS), $Fe(NO_3)_3.9H_2O$ (98%, Fisher Scientific) and $(NH_4)_2HPO_4$ (98%, Merck) were dissolved in de-ionised water separately and then mixed together to have a final precursor solution having a pH value of 2. This solution was placed on a hot plate (maintained at 120 °C) with steady magnetic stirring to remove excess water. After complete drying, the solid residue was ground by an agate mortar and pestle was pressed into pellets using hydraulic press. These pellets were calcined in a tubular furnace at 400 °C for 6 h, 600 °C for 6 h and finally at 750 °C for 48 h to get the final product. This annealing condition was used for precursor mixture without using any fuel. In contrast, when fuels were mixed to precursor solution, the desired product was obtained by one-step calcination at 750 °C for 6 h. A fire yellow coloured powder was finally obtained.

2.2. Structure and morphological analysis

The powder diffraction patterns of $Na_3Fe_3(PO_4)_4$ samples were acquired by a PANalytical X'Pert Pro diffractometer equipped with a Cu-Kα source ($\lambda_1 = 1.5405$ Å, $\lambda_2 = 1.5443$ Å) operating at 40 kV/30 mA. Typical XRD patterns were collected using Bragg–Brentano geometry in the 2θ window of 5°–90° with a step size of 0.0267° (count time = 110 s per step). Synchrotron diffraction pattern was collected at the BL-18B Indian beamline (High Energy Accelerator Research Organization, KEK-Photon Factory, Tsukuba, Japan) using a synchrotron beamline of wavelength $\lambda = 0.7861(2)$ Å and energy E = 15.77 keV calibrated with Si (640b NIST) standard. Neutron powder diffraction (NPD) pattern was acquired with Echidna high-resolution diffractometer at OPAL facility (Lucas Heights, Australia) using neutrons of wavelength 2.4395 Å. Rietveld analysis of the powder diffraction patterns was conducted using GSAS [17, 18] or FullProf [19] suite of programs. The background was refined using a shifted Chybeshev polynomial function and the diffraction profile was fitted by a pseudo-Voigt function. Brunauer-Emmett-Teller (BET) surface area measurements were calculated with a Micromeritics ASAP 2020 instrument using surface adsorption of N_2 (at 77 K). Prior to BET test, the powder samples were evacuated at 373 K under vacuum for 2 h. The morphology of as-synthesized product was examined using an FEI Inspect F50 scanning electron microscope (10 kV) as well as an FEI Tecnai F30 STwin transmission electron microscope (200 kV). For TEM analysis, few drops of powder sample, soaked in acetone, were deposited on a copper grid.

2.3. Magnetic characterization

Temperature-dependent magnetic susceptibility data over a 4–300 K range were collected for $Na_3Fe_3(PO_4)_4$ under field-cooled (FC) and zero field-cooled (ZFC) conditions, in an applied magnetic field of 1000 Oe. Field-dependent data were collected at 4 K over the range ±5000 Oe. Measurements were made using a Quantum

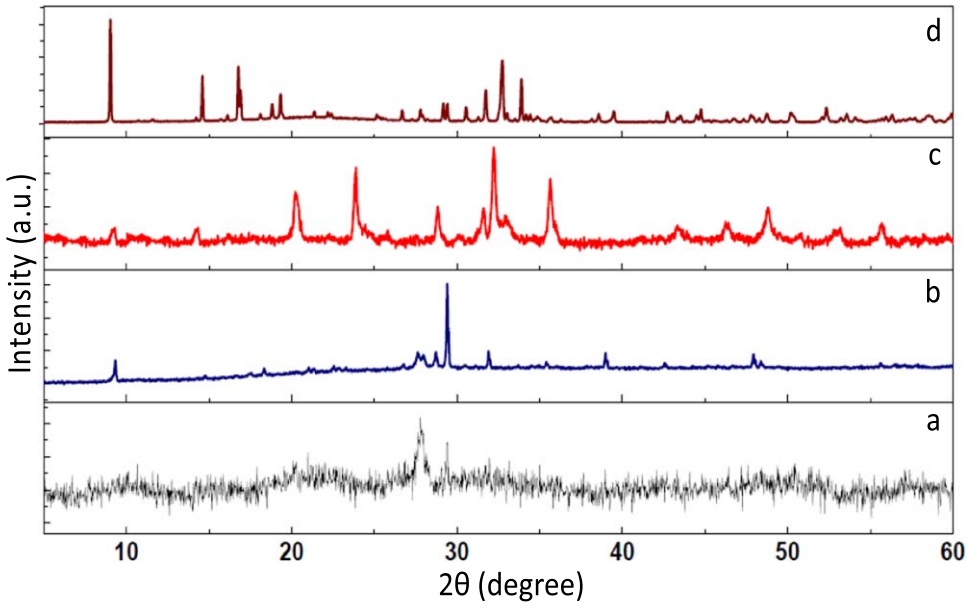

Figure 1. Comparative X-ray diffraction patterns elucidating the evolution of $Na_3Fe_3(PO_4)_4$ product phase obtained by solvothermal synthesis without any fuel. XRD patterns are shown for (a) intermediate product obtained after dehydration and its derivative products after (b) one step calcination at 400 °C for 6 h, (c) two step calcination at 400 °C for 6 h followed by 600 °C for 6 h and (d) three step calcination at 400 °C for 6 h followed by 600 °C for 6 h with final calcination at 750 °C for 48 h.

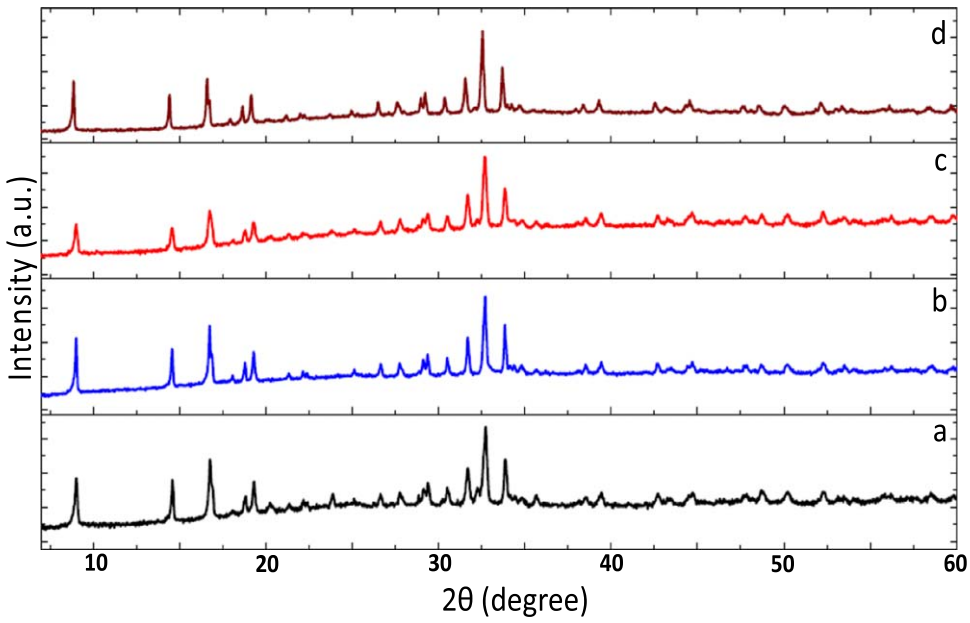

Figure 2. Solvothermal synthesis of $Na_3Fe_3(PO_4)_4$ product phase with one step calcination at 750 °C for 6 h using various fuels like (a) urea, (b) glycine, (c) ascorbic acid and (d) no fuel. The corresponding surface area values are provided in table 2.

Design Physical Property Measurement System (PPMS) equipped with a Vibrating Sample Magnetometer (VSM).

2.4. Electrochemical characterization

The electrochemical properties of $Na_3Fe_3(PO_4)_4$ were tested (at 25 °C) in sodium half-cell architectured CR2032 coin type cells. Composite positive electrode (slurry) was prepared by thoroughly mixing the active material (85 wt%) with carbon black (10 wt%) and polyvinylidene fluoride binder (5 wt%) in N-methyl-pyrrolidone. The slurry was coated uniformly with brush onto thin circular Al-foil ($\varnothing = 16$ mm) and was dried overnight in vacuum oven at 90 °C. The coin cells were assembled in an argon-filled glove box (MBraun Inc.) using Na metal

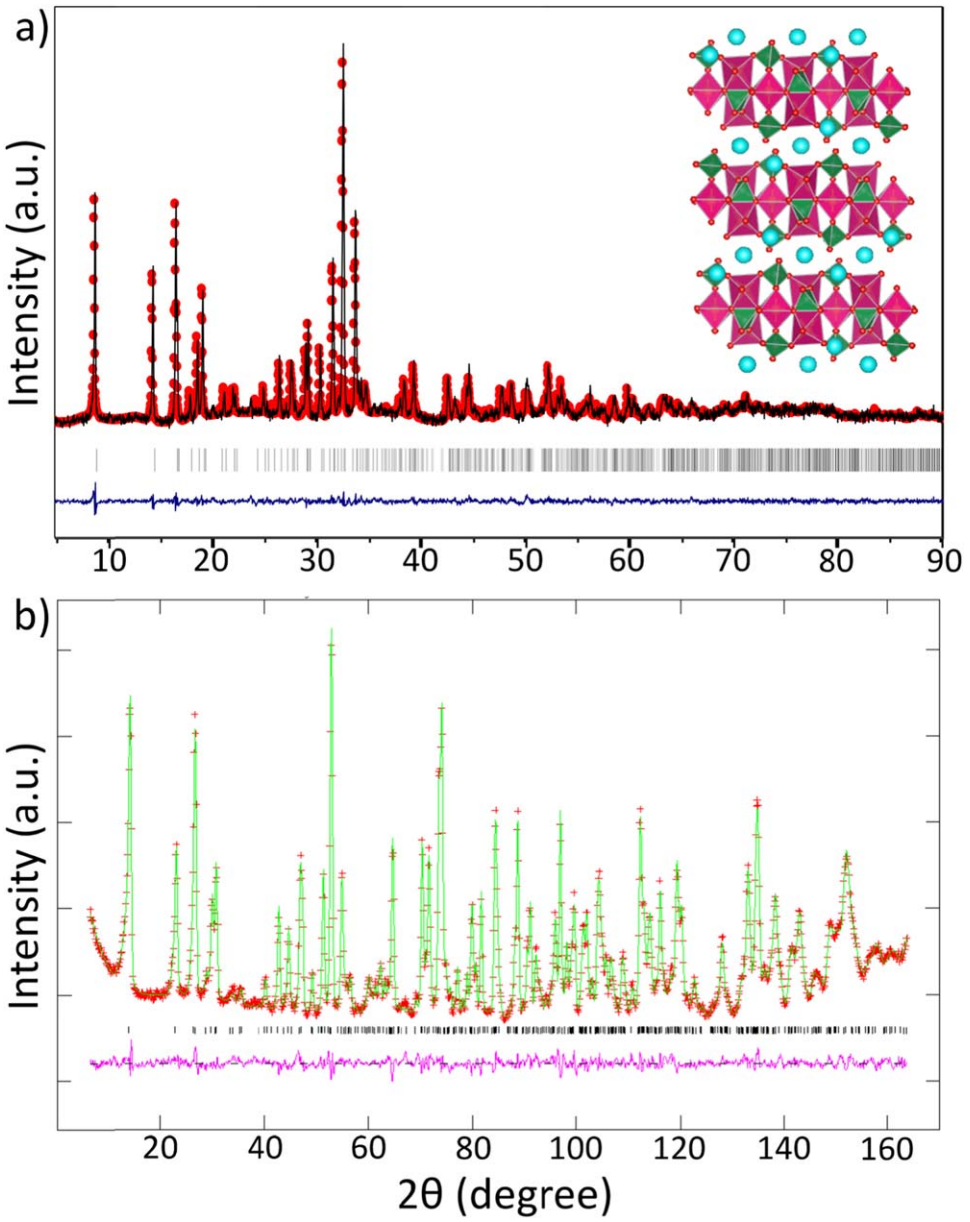

Figure 3. (a) Rietveld refined X-ray powder pattern of $Na_3Fe_3(PO_4)_4$ product showing the experimental data points (red), calculated pattern (black), their difference (blue) and Bragg diffraction peaks (black ticks). (Inset) Illustration of $Na_3Fe_3(PO_4)_4$ framework built with interconnected FeO_6 octahedra (pink) and PO_4 tetrahedra (green) with large cavities accommodating the Na atoms (blue). (b) Rietveld refined neutron diffraction pattern ($\lambda = 2.4395$ Å) of $Na_3Fe_3(PO_4)_4$.

foils as counter electrode and a sheet of Whatman filter paper as separator soaked with 1.0 mol.l^{-1} $NaClO_4$ in propylene carbonate as electrolyte. These cells were galvanostatically cycled between 2–2.55 V (versus Na/Na^+) at a rate of C/50 (i.e. 1 Na in 50 h at 25 °C) using a VMP3 Biologic battery cycler.

3. Results and discussion

3.1. Synthesis and structure

Phosphate based compounds are important among the polyanionic insertion materials as they are durable over high temperature and provides more chemical stability along with good electrochemical properties. From elemental point of view, Fe-based cathodes are projected as economic candidates due to the abundance of Fe-based precursors. Nonetheless, the processing cost plays the spoiler as most Fe-based cathode materials are based on Fe^{2+} species warranting careful processing and packaging in inert (N_2/Ar) atmosphere. Switching towards Fe^{3+} based cathode materials [like layered $Na_3Fe_3^{3+}(PO_4)_4$] can reduce the processing cost ($/watt-hour) of material as whole process can be carried in air instead of inert (Argon) atmosphere. Also, conventional

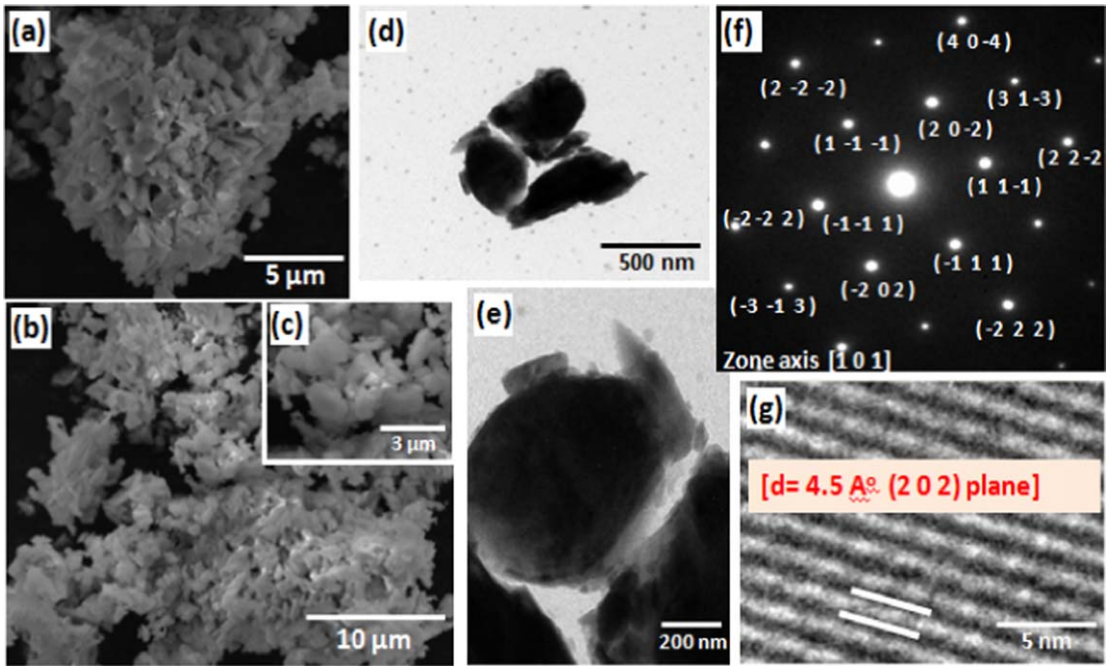

Figure 4. Electron micrographs illustrating the particle morphology. (a)–(c) SEM images, (d), (e) TEM images, (f) selected area diffraction pattern with indexing, and (g) representative HRTEM image showing the lattice fringes.

Table 1. Crystallographic structure parameters of $Na_3Fe_3(PO_4)_4$ calculated from Rietveld analysis of neutron powder diffraction ($\lambda = 2.4395$ Å) at 25 °C.

Formula [molecular weight]	$Na_3Fe_3(PO_4)_4$ [616.39] ($Z = 4$)
Crystal system	Monoclinic
Space group	$C2/c$ (#15)
Unit cell parameters (Å)	$a = 19.5552(16)$, $b = 6.3858(5)$, $c = 10.5712(9)$ Unique angle $\beta = 91.7447(20)°$
Unit cell volume (Å^3)	1319.48(32)
Fitness parameters	$Rp = 2.72$, $R_{wp} = 3.46$, $R_{exp} = 2.0$, $\chi^2 = 3.0$

Atom	Site	x	y	z	Occupancy	U_{iso} (Å^2)	BVS
Na1	4e	0	0.3652(24)	1/4	1	0.008(4)	0.952
Na2	8 f	0.0838(6)	0.1441(16)	0.9748(10)	1	0.0050(31)	0.942
Fe1	4d	1/4	1/4	1/2	1	0.0025(19)	3.267
Fe2	8 f	0.15615(19)	0.4762(7)	0.7470(4)	1	0.0004(11)	3.109
P1	8 f	0.2022(4)	0.0205(12)	0.2431(6)	1	0.0019(7)	4.856
P2	8 f	0.9131(4)	0.3377(11)	0.0109(7)	1	0.0019(7)	4.904
O1	8 f	0.15897(30)	0.8306(11)	0.2748(6)	1	0.0019(7)	1.955
O2	8 f	0.25639(34)	0.0570(9)	0.3539(7)	1	0.0019(7)	2.122
O3	8 f	0.15826(32)	0.2084(11)	0.2126(6)	1	0.0019(7)	1.866
O4	8 f	0.25427(32)	0.9762(10)	0.1338(6)	1	0.0019(7)	1.920
O5	8 f	0.91589(33)	0.4598(10)	0.8801(6)	1	0.0019(7)	1.945
O6	8 f	0.9036(4)	0.5130(11)	0.1128(6)	1	0.0019(7)	2.139
O7	8 f	0.97486(34)	0.2073(10)	0.0389(6)	1	0.0019(7)	1.980
O8	8 f	0.84857(35)	0.2030(10)	0.0073(7)	1	0.0019(7)	1.995

solid-state synthesis involves high temperature and prolonged calcination time which augment the processing cost of material. In search of alternative novel synthesis, wet-synthesis and solution combustion synthesis involving short calcination duration can be employed for scalable production of variety of cathode materials. Here, (fuel-assisted) solvothermal route was employed for energy-savvy synthesis of layered $Na_3Fe_3(PO_4)_4$.

Without any fuel, wet synthesis was conducted involving multi-step calcination at 400 °C and 600 °C for 6 h followed by final heat treatment at 750 °C for 48 h. The phase evolution with various calcination steps is depicted

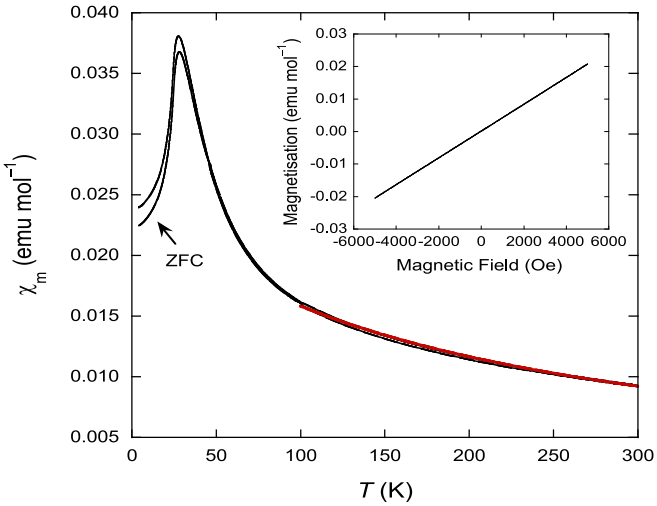

Figure 5. Field-cooled and zero field-cooled magnetic susceptibility for $Na_3Fe_3(PO_4)_4$ in an applied field of 1000 Oe. The red line is a fit to the Curie-Weiss las over the range 100–300 K. The inset shows the field dependent magnetic susceptibility at 4 K.

Table 2. BET surface area and BJH pore size measurements for $Na_3Fe_3(PO_4)_4$ samples prepared by solvothermal synthesis using various fuels.

Fuel used	BET Specific Surface area ($m^2\ g^{-1}$)	BJH desorption average pore size (nm)
Without fuel	2.124	13.6751
Ascorbic acid ($C_6H_8O_6$)	2.961	16.3634
Glycine ($C_2H_5NO_2$)	2.605	17.9311
Urea (CH_4N_2O)	2.292	21.6622

in figure 1. While the intermediate product (after dehydration) was amorphous in nature, progressive phase evolution occurred with high temperature annealing. Usage of wet synthesis favouring intimate mixing of precursors led to reduction of final annealing duration from (previously reported) 72 h to 48 h [14, 15]. Faster reaction can be realized by triggering exothermic combustion reaction in presence of fuels that leads to intimate precursor mixing/metal-nitrate complexation, exothermic reaction involving high local heating, rapid product formation with porous (nanoscale) morphology along with one-step carbon coating [20, 21]. When combustion synthesis was employed, facilitated by complexation and partial reaction completion during low temperature step, the final calcination duration (at 750 °C) was drastically reduced to 6 h independent of the fuels used (figure 2). Structural and phase purity was analysed combining lab/synchrotron XRD and neutron powder diffraction. Rietveld refinement confirmed the formation of desired target product as shown in figure 3. No trace of possible impurity like *maricite* $NaFePO_4$ or $NaFeP_2O_7$ was noticed. The structure could be indexed to monoclinic framework with $C2/c$ symmetry. The unit cell parameters and atomic coordinates derived from Rietveld analysis of neutron powder diffraction pattern are summarized in table 1. The calculated BVS values are close to the valency of respective elements.

Layered $Na_3Fe_3(PO_4)_4$ structure is illustrated in the inset of figure 3. The framework consists of FeO_6 octahedral and PO_4 tetrahedral building blocks. While adjacent FeO_6 octahedra are solely connected by corner-sharing arrangement, they are abridged by PO_4 tetrahedra involving both corner-sharing and edge-sharing fashion. Fe occupies two distinct crystallographic sites. While Fe(1)–O_6 shares oxygen atoms solely by corner-sharing fashion, the Fe(2)–O_6 involves both corner and edge sharing bonding with PO_4 tetrahedra. Owing to the size difference between FeO_6 and PO_4 units, FeO_6–PO_4 edge sharing leads to distortion of Fe(2)–O_6 octahedra. The constituent Na atoms are located in between the FeO_6–PO_4 layers having two distinct crystallographic sites, a six-coordinated Na(1)–O_6 and a seven-coordinated Na(2)–O_7 sites, creating three-dimensional Na^+ diffusion pathways along [010], [110] and [1–10] directions.

The solvothermally prepared $Na_3Fe_3(PO_4)_4$ consists of micrometric (1–3 μm) anisotropic platelets which forms large agglomerates (figures 4(a)–(c)). This aggressive grain growth and large particle size results from prolonged thermal treatment. BET analysis revealed the overall surface area to be in the range of 2–3 $m^2\ g^{-1}$ with

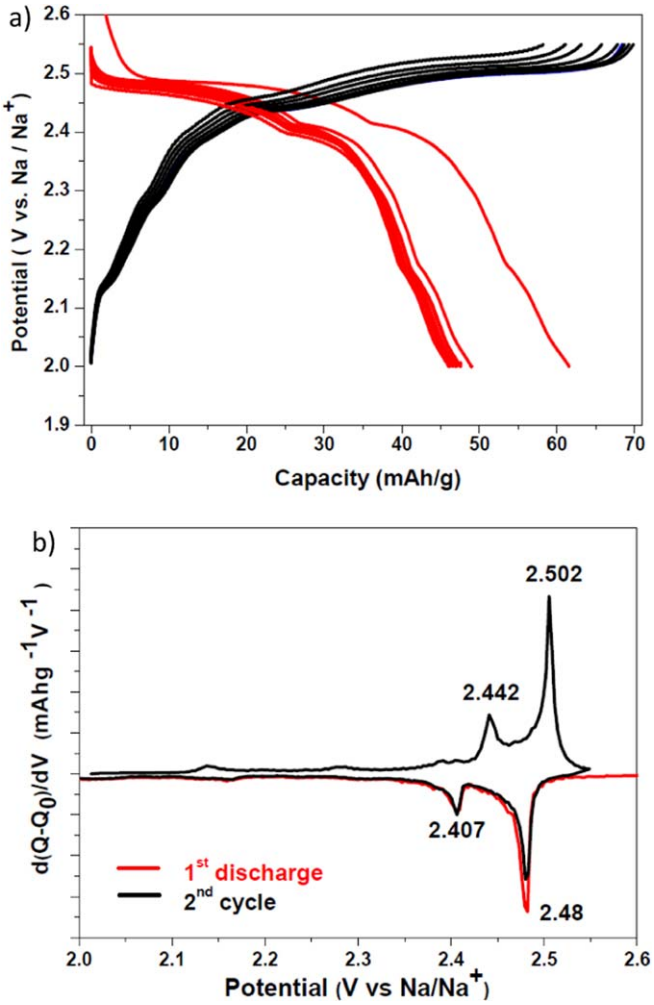

Figure 6. (a) Galvanostatic charge-discharge voltage profiles of $Na_3Fe_3(PO_4)_4$ cathode (versus Na) cycled in the potential window of 2–2.55 V at the rate of C/50 (at 25 °C) for the initial 10 cycles. (b) Corresponding differential capacity (dQ/dV) profile.

mesoporous morphology (pore size: 13–22 nm) (table 2). High-resolution TEM study further confirmed the formation of inhomogeneous micrometric $Na_3Fe_3(PO_4)_4$ particles in the size range of 1–2 μm (figures 4(d)–(e)). SAED pattern could be indexed to monoclinic structure (figure 4(f)). The crystallinity of final product was further confirmed by HRTEM study showing lattice planes corresponding to miller indices (202) with an interatomic *d*-spacing of 4.5 Å (figure 4(g)).

3.2. Magnetic properties

The presence of Fe imparts magnetic characteristic to $Na_3Fe_3(PO_4)_4$, similar to many Fe-based cathode materials with antiferromagnetic ordering at low temperature. Temperature-dependent magnetic susceptibility data for $Na_3Fe_3(PO_4)_4$ under field-cooled (FC) and zero field-cooled (ZFC) conditions are presented in figure 5. An antiferromagnetic ordering transition is clearly observed at $T_N = 27$ K. There was no significant offset between the FC and ZFC data, consistent with the absence of any opening in the field-dependent data at 4 K (inset to figure 5). A Curie-Weiss fit to the FC data over the range 100–300 K (red line in figure 5) yields an effective magnetic moment $\mu_{eff} = 5.95\ \mu_B$/Fe, consistent with the theoretical spin-only value for high-spin Fe^{3+}, $\mu_{s.o.} = 5.92\ \mu_B$/Fe. A detailed analysis of long range magnetic ordering and elucidation of antiferromagnetic structure of $Na_3Fe_3(PO_4)_4$ from low-temperature neutron diffraction data will be reported shortly.

3.3. Electrochemical performance of $Na_3Fe_3(PO_4)_4$

Electrochemical performance of wet chemistry prepared $Na_3Fe_3(PO_4)_4$ was analysed using standard Na half-cell assembly. Being an Fe^{3+} insertion compound, $Na_3Fe_3(PO_4)_4$ was first discharged to uptake further Na atoms to realize Fe^{3+}/Fe^{2+} redox activity. Ideally, it will be great to utilize Fe^{3+}/Fe^{4+} redox activity by charging (desodiating) the starting compound. However, the reversible conversion of Fe^{3+}–Fe^{4+} involving FeO_6 octahedral environment is structurally unstable and this redox can occur beyond safe operation limit of

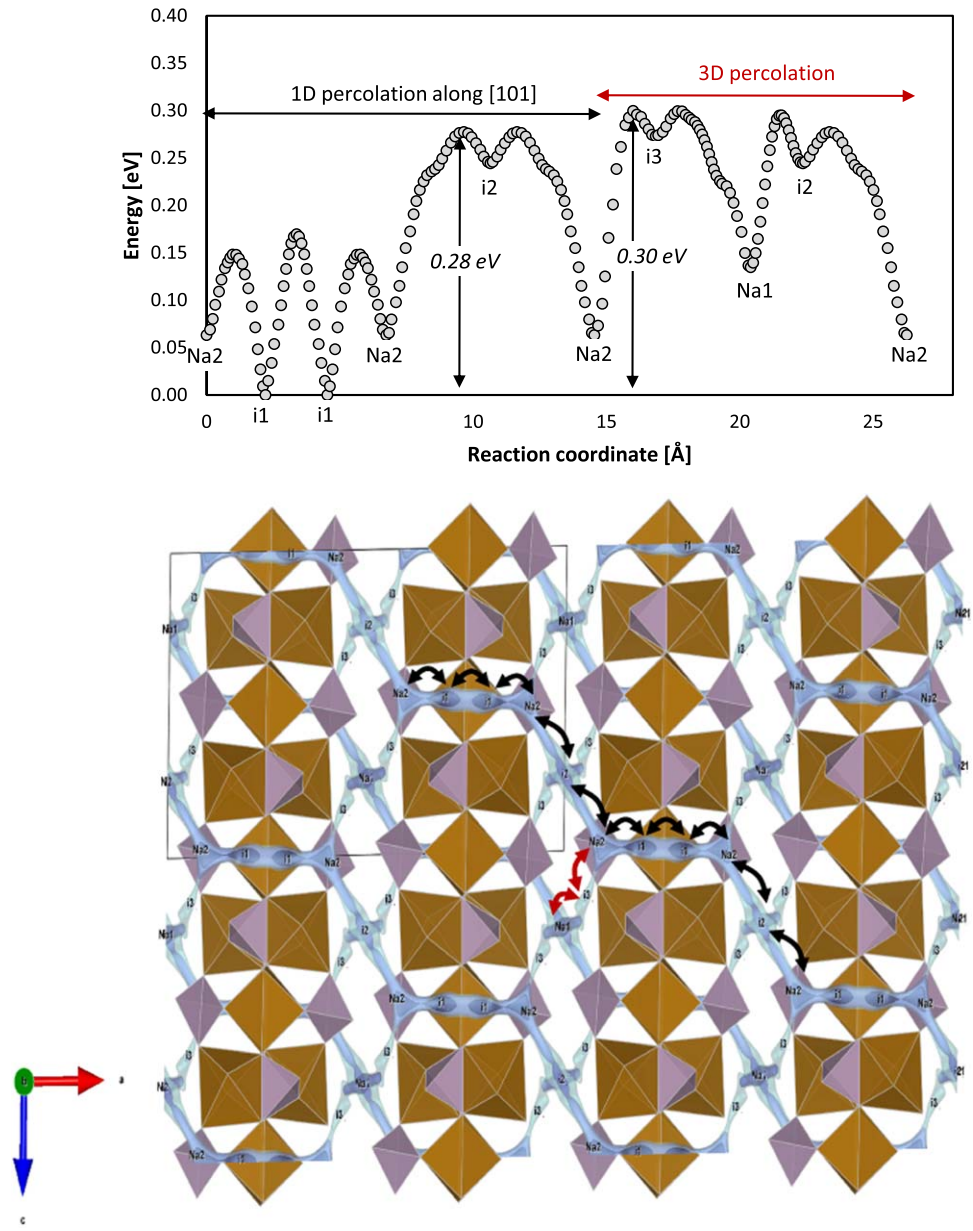

Figure 7. (a) Migration energy barrier profile for Na^+ diffusion in $Na_3Fe_3(PO_4)_4$ as derived from the bond valence site energy (BVSE) model. (b) Na^+ pathways with interstitial sites in $Na_3Fe_3(PO_4)_4$ displayed as isosurfaces of constant $E_{BVSE}(Na)$ superimposed on a projection of the crystal structure along *ac* plane. Black arrows show one possible dimensional hopping pathway while red arrow indicates three-dimensional hopping pathway Na^+ diffusion.

commonly used electrolytes. Galvanostatic voltage-capacity profiles of layered $Na_3Fe_3(PO_4)_4$ is shown in figure 6(a). When tested at a rate of C/50 (1 Na^+ in 50 h), the first discharge capacity of 66 mAh g^{-1} was observed (theoretical capacity ~130 mAh g^{-1}). In subsequent cycles, ~1.6 Na^+ ions could be reversibly inserted into the structure delivering a discharge capacity ~48 mAh g^{-1}. Similar to many polyanionic cathodes (like $Li_2FeP_2O_7$), the capacity decreased from 1st to 2nd cycle hinting at irreversible structural rearrangement during the first discharge. Afterwards, the cell performed with steady capacity (ca. 48 mAh g^{-1}) with 98% Coulombic efficiency. A closer look revealed sloping step-wise profiles with several distinct pseudo-plateaus. The major Fe^{3+}/Fe^{2+} redox peak appears ~2.5 V followed by several minor redox peaks ~2.42 V and 2.14 V (vs. Na/Na^+) (figure 6(b)). This sloping profile is indicative of solid-solution (single-phase) redox mechanism during (de) sodiation reaction. While the original report involving prolonged solid-state synthesis showed poor electrochemical activity even at a slow rate of C/100 [14, 15], the usage of solvothermal synthesis (delivering smaller particles) led to similar electrochemical performance at improved rate of C/50. Nonetheless, layered $Na_3Fe_3(PO_4)_4$ is found to have poor Na^+ diffusion despite all attempts on processing/material optimization.

To understand the reason behind poor electrochemical activity in $Na_3Fe_3(PO_4)_4$, the Na^+ diffusional kinetics and pathways were explored using bond valence site energy (BVSE) calculations, which is a simple yet

reliable approach to speculate ion migration pathways in structural models. The detail methodology of BVSE analysis has been reported elsewhere [22–24]. In this calculations, the bond valences $s_{Na-X} = \exp[(R_{0,Na-X} - R_{Na-X})/b_{Na-X}]$ and the BV sum mismatch $|\Delta V|$ can be correlated to an absolute energy scale by expressing the bond valence site energy E_{BVSE} of a Na^+ cation coordinated by X^- anions as a Morse-type interaction energy:

$$E_{BVSE}(Na) = \sum_x D\left[\sum_{i=1}^{N}\left(\left(\frac{s_{Na-X}}{s_{\min,Na-X}}\right)^2 - 2\frac{s_{Na-X}}{s_{\min,Na-X}}\right)\right] + E_{repulsion}$$

The required bond valence parameters were taken from *softBV* database [25]. Migration pathways for Na^+ are then investigated as regions of low bond valence site energy E_{BVSE}(Na) in grids spanning the structure model with a resolution of ca. $(0.1\ Å)^3$. Using Rietveld refinement of neutron diffraction of $Na_3Fe_3(PO_4)_4$ sample, the initial structure model was obtained for BVSE calculations. Based upon structure model, energy barrier for Na^+ migration as hollow spheres connecting the Na and interstitial sites in $Na_3Fe_3(PO_4)_4$ was obtained and represented as superimposed projection of the crystal structure along *ac* plane in figure 7. $Na_3Fe_3(PO_4)_4$ has two sites for Na (Na1 and Na2), where Na2 has lowest energy barrier of 0.15 eV for hopping to other Na2 via the interstitial sites *i*1- *i*1 with hopping energy barrier of 0.17 eV as illustrated in figure 7 (top). Hopping of Na2 also takes place from *i*2 interstitial site with high energy barrier of 0.28 eV along one dimensional pathway to Na2. Three-dimensional percolation of Na2 is possible involving Na1 with highest migration energy barrier of 0.30 eV from the interstitial sites *i*3 site. Using VETSA, one-dimensional as well as three-dimensional percolation pathways are superimposed over crystal structure of $Na_3Fe_3(PO_4)_4$ along *ac* plane as shown in figure 7 (bottom). Migration of Na in $Na_3Fe_3(PO_4)_4$ follows one-dimensional pathway along Na2-*i*1-*i*1-Na2 (figure 7 black arrows) which are more feasible than three-dimensional percolation pathway along Na2-*i*3-Na1 due less energy barrier (figure 7 red arrows). Overall, it offers feasible one-dimensional Na^+ diffusivity with high energy barrier, which is the root cause behind the poor rate kinetics in this system.

4. Conclusions

This work presents the first wet chemistry synthesis and layered sodium iron phosphate $Na_3Fe_3(PO_4)_4$ insertion system. Using this solvothermal synthesis, the target compound was prepared by less aggressive heat treatment resulting subdued grain growth/Ostwald ripening vis-à-vis solid-state synthesis. Rietveld analysis confirmed the formation of monoclinic layered system. Microstructural analysis showed large agglomerated platelets of 5–7 μm range with primary anisotropic platelet shaped particles in the size range of 1–2 μm. It exhibited a long-range antiferromagnetic ordering below (T_N=) 27 K. Wet synthesis improved the Na^+ diffusion kinetics in $Na_3Fe_3(PO_4)_4$ when tested in sodium cells. Involving a nominal Fe^{3+}/Fe^{2+} redox potential centred around 2.43 V, it delivered a reversible capacity of 48 mAh g^{-1}. The poor Na^+ insertion behaviour in $Na_3Fe_3(PO_4)_4$ can be rooted to structural disordering during initial cycle and occurrence of one-dimensional Na^+ diffusion pathways along [101] direction with high energy barrier of 0.28 eV. While far from any practical application, $Na_3Fe_3(PO_4)_4$ forms an economic Fe^{3+}-based sodium insertion material.

Acknowledgments

P B thanks the Department of Atomic Energy (DAE) for a DAE-BRNS Young Scientists Research Award (YSRA). R G is grateful to ICDD for a Ludo-Frevel Crystallography Scholarship and ECS for an FM Becket Summer Fellowship. S A and R P R are grateful to National Research Foundation, Prime Minister's Office, Singapore for support under the Competitive Research Programme (CRP Award NRF-CRP 10-2012-6) and acknowledge support from the NUS 'Centre for Energy Research' seed grant. M A and C D L acknowledge the financial support from the Australian Research Council (DP170100269).

ORCID iDs

Ritambhara Gond https://orcid.org/0000-0003-3061-7434
Maxim Avdeev https://orcid.org/0000-0003-2366-5809
Chris D Ling https://orcid.org/0000-0003-2205-3106
Rayavarapu Prasada Rao https://orcid.org/0000-0002-4022-2340
Stefan Adams https://orcid.org/0000-0003-0710-135X
Prabeer Barpanda https://orcid.org/0000-0003-0902-3690

References

[1] Goodenough J B and Park K S 2013 The Li-ion rechargeable batteries: a perspective *J. Am. Chem. Soc.* **135** 1167
[2] Larcher D and Tarascon J M 2015 Towards greener and more sustainable batteries for electrical energy storage *Nat. Chem* **7** 19
[3] Braconnier J J, Delmas C, Fouassier C and Hagenmuller P 1980 Comportement electrochemique des phases Na_xCoO_2 *Mater. Res. Bull.* **15** 1797
[4] Delmas C, Braconnier J J, Fouassier C and Hagenmuller P 1981 Electrochemical intercalation of sodium in Na_xCoO_2 bronzes *Solid State Ionics* **3–4** 165
[5] Xia X and Dahn J R 2012 $NaCrO_2$ is a fundamentally safe positive electrode material for sodium-ion batteries with liquid electrolytes *Electrochem. Solid-State Lett.* **15** A1
[6] Yabuuchi N, Kubota K, Dahbi M and Komaba S 2014 Research development of sodium-ion batteries *Chem. Rev.* **114** 11636
[7] Yabuuchi N, Kajiyama M, Iwatate J, Nishikawa H, Hitomi S, Okuyama R, Usui R, Yamada Y and Komaba S 2012 P2-type $Na_x[Fe_{1/2}Mn_{1/2}]O_2$ made from earth-abundant elements for rechargeable Na batteries *Nat. Mater.* **11** 512
[8] Yabuuchi N and Komaba S 2014 Recent research progress on iron- and manganese-based positive electrode materials for rechargeable sodium batteries *Sci. Technol. Adv. Mater.* **15** 043501
[9] Padhi A K, Manivannan V and Goodenough J B 1998 Tuning the position of redox couples in materials with NASICON structure by anionic substitution *J. Electrochem. Soc.* **145** 1518
[10] Barpanda P 2016 Pursuit of sustainable iron-based sodium battery cathodes: two case studies *Chem. Mater.* **28** 1006
[11] Barpanda P, Oyama G, Nishimura S, Chung S C and Yamada A 2014 A 3.8 V earth-abundant sodium battery electrode *Nat. Commun.* **5** 4358
[12] Dwibedi D, Ling C D, Araujo R B, Chakraborty S, Duraisamy S, Munichandraiah N, Ahuja R and Barpanda P 2016 Ionothermal synthesis of high-voltage alluaudite $Na_{2+2x}Fe_{2-x}(SO_4)_3$ sodium insertion compound: structural, electronic and magnetic insights *ACS Appl. Mater. Interfaces.* **8** 6982
[13] Barpanda P, Liu G, Ling C D, Tamaru M, Avdeev M, Chung S C, Yamada Y and Yamada A 2013 $Na_2FeP_2O_7$: a safe cathode for rechargeable sodium-ion batteries *Chem. Mater.* **25** 3480
[14] Trad K, Carlier D, Croguennec L, Wattiaux A, Lajmi B, Amara M B and Delmas C 2010 A layered iron(III) phosphate phase, $Na_3Fe_3(PO_4)_4$: synthesis, structure and electrochemical properties as positive electrode in sodium batteries *J. Phys. Chem.* C **114** 10034
[15] Trad K, Carlier D, Wattiaux A, Amara M B and Delmas C 2010 Study of a layered iron(III) phosphate phase $Na_3Fe_3(PO_4)_4$ used as positive electrode in lithium batteries *J. Electrochem. Soc.* **157** A947
[16] Lajmi B, Hidouri M, Rzeigui M and Amara M B 2002 Reinvestigation of the binary diagram Na_3PO_4–$FePO_4$ and crystal structure of new iron phosphate $Na_3Fe_3(PO_4)_4$ *Mater. Res. Bull.* **37** 2407
[17] Rietveld H M 1969 A profile refinement method for nuclear and magnetic structures *J. Appl. Cryst.* **2** 65
[18] Larson A C and Von Dreele R B 1994 General structure analysis system (GSAS) Los Alamos National Laboratory Report, LAUR 86-748, Los Alamos National Laboratory Los Alamos, NM
[19] Rodriguez-Carvajal J M 1993 Recent advances in magnetic structure determination by neutron powder diffraction *Phys.* B **192** 55
[20] Gond R, Meena S S, Yusuf S M, Shukla V, Jena N K, Ahuja R, Okada S and Barpanda P 2017 Enabling the electrochemical activity in sodium iron metaphosphate $[NaFe(PO_3)_3]$ sodium battery insertion material: structural and electrochemical insights *Inorg. Chem.* **56** 5918
[21] Sharma L, Nayak P K, de la Llave E, Chen H, Adams S, Aurbach D and Barpanda P 2017 Electrochemical and diffusional investigation of $Na_2Fe^{II}PO_4F$ fluorophosphate sodium insertion material obtained from Fe^{III} precursor *ACS Appl. Mater. Interfaces.* **9** 34961
[22] Adams S and Prasada Rao R 2014 *Bond Valences* ed I D Brown and K R Poeppelmeier (Berlin: Structure and Bonding Springer) 158, 129
[23] Adams S and Prasada Rao R 2011 Simulated defect and interface engineering for high power Li electrode materials *Solid State Ionics* **184** 57
[24] Adams S and Prasada Rao R 2009 Transport pathways for mobile ions in disordered solids from the analysis of energy-scaled bond-valence mismatch landscapes *Phys. Chem. Chem. Phys.* **11** 3210
[25] Chen H and Adams S 2017 Bond softness sensitive bond-valence parameters for crystal structure plausibility tests *IUCr J.* **4** 614